ISSN 1990-3413, Astrophysical Bulletin, 2017, Vol. 72, No. 2, pp. 150–164. © Pleiades Publishing, Ltd., 2017.
Original Russian Text © O.P. Zhelenkova, N.S. Soboleva, A.V. Temirova, N.N. Bursov, 2017, published in Astrofizicheskii Byulleten', 2017, Vol. 72, No. 2, pp. 166–182.

Deep 7.6 cm RATAN-600 Sky Surveys at the Declination of SS 433 During the 1980–1999 Period. Catalog of Radio Sources in the Right-Ascension Interval $2^h \leq \mathrm{RA} < 7^h$

O. P. Zhelenkova[1,2*], N. S. Soboleva[†3], A. V. Temirova[3], and N. N. Bursov[1]

[1] *Special Astrophysical Observatory, Russian Academy of Sciences, Nizhnii Arkhyz, 369167 Russia*
[2] *ITMO University, St. Petersburg, 197101 Russia*
[3] *St. Petersburg Branch of the Special Astrophysical Observatory of the Russian Academy of Sciences, St. Petersburg, 196140 Russia*

Received January 11, 2017; in final form, March 20, 2017

Abstract—We present a catalog of radio sources extending the RCR (RATAN Cold Refined) catalog to the right-ascension interval $2^h \leq \mathrm{RA} < 7^h$. The list of objects was obtained in the process of a reprocessing of the observations of the "Cold" experiment conducted in 1980–1981 on RATAN-600 radio telescope at the declination of SS 433, and the reduction of the 1987–1999 surveys of the same experiment. We report the right ascensions and integrated flux densities for 237 sources found at 7.6 cm (3.94 GHz) and their spectral exponents at 3.94 and 0.5 GHz. Twenty-nine sources of the list, which are mostly weaker than 30 mJy at 3.94 GHz, have available data only at two frequencies—1.4 and 3.94 Hz. We approximated the spectra of the sources using all catalogs available in the CATS and VizieR databases that meet the survey strip, and, in some cases, using the flux densities estimates from VLSSr, GLEAM, TGSS, and GB6 survey maps. We constructed the histograms of the spectral indices of the sources and verified the reliability of the identifications of sources found in the scans by comparing the coordinates and integrated flux densities with the corresponding parameters listed in the NVSS catalog. In the right ascension interval considered we found no objects at the 10–15 mJy level lacking in decimeter-wave catalogs.

DOI: 10.1134/S1990341317020067

Key words: *radio continuum: general*

1. INTRODUCTION

In 1991 the RC (RATAN Cold) [1] catalog was published featuring 7.6 cm integrated flux densities for objects in the $4^h \leq \mathrm{RA} < 22^h$ in the declination strip $\mathrm{Dec}_{1980} = 4^\circ57' \pm 20'$ ($\mathrm{Dec}_{2000} = 4^\circ59' \pm 20'$). The catalog is based on the results of observations carried out in 1980–1981 on RATAN-600 radio telescope at the meridian and at the azimuth of 30° within the framework of the "Cold" experiment [2–4]. The coordinate calibrations of the scans was based on UTRAO (365 MHz) used as the reference catalog whose data for the sky strip considered were kindly provided by Professor G. N. Douglas before the publication of the catalog.

After the publication of the 1.4 GHz NVSS [5] and FIRST [6] surveys of higher coordinate accuracy and sensitivity compared to UTRAO the RC catalog was compared to these data and it was shown that about one fourth of RC sources could not be identified with NVSS [7, 8]. This is due, among other factors, to the fact that the beam pattern (BP) of the radio telescope is elongated in the altitude, making identification of objects found in the scan difficult in the cases where several sources located within the field of view are convolved with such an extended BP. Second: bright sources, which during the transit are located far from the central cross section of the BP, may cause the detection of false sources by the side lobes.

From 1987 to 1999 several observing runs were carried out at the meridian on the Northern sector of RATAN-600 within the framework of the "Cold" experiment. These data were used to refine the flux densities and coordinates of the sources of the RC catalog. For the discussion of the results obtained for observations carried out in the right-ascension interval $2^h \leq \mathrm{RA} < 7^h$ and $17^h \leq \mathrm{RA} < 22^h$ see Soboleva et al. [9] (the catalog of the sources found was not published in the above paper). The observational data of the 1980–1999 surveys in the right-ascension

[†] Deceased.
[*] E-mail: zhe@sao.ru

interval $7^h \leq RA < 17^h$ were later rereduced and the results of this reduction were published as the RCR (RATAN Cold Revised) catalog [10].

In this paper we publish the list of sources found during the reduction of 1987–1999 observations made at 7.6 cm (3.94 GHz) and rereduction of the scans obtained in 1980 in the right-ascension interval $2^h \leq RA < 7^h$.

We identified all detected sources with NVSS sources and used NVSS catalog for right-ascension calibration. We did not determine the declinations of the sources and adopted the declinations of NVSS objects.

We used Aladin software [11, 12] and TOPCAT tool for working with tables and catalogs [13] for cross identifying our sources with NVSS and other digital surveys.

Here we report the list of sources detected on averaged scans. It extends the RCR catalog to the right-ascension interval $2^h \leq RA < 7^h$.

The paper is structured as follows: Section 2 describes the reduction of observations; Section 3 describes the table with the resulting list; Section 4 presents an analysis of the spectra of RCR sources, and in Section 5 we discuss the reliability of the identification of sources by comparing the right ascensions and integrated flux densities determined from averaged scans with the NVSS catalog and estimate the area covered by the catalog.

2. REDUCTION OF OBSERVATIONS

We reduced 7.6 cm observations using standard reduction methods. For a detailed description of the reduction technique see Soboleva et al. [14]. We smoothed the averaged scans by folding them with the computed beam pattern in its central cross section. We then determined the background level with the 20 s "smoothing window" and used Gaussian analysis to identify sources in the scan. Time calibration was based on strong NVSS sources.

For each detected radio source we determined its position in the scan (RA), antenna temperature (T_a), and the half-width of the power beam pattern ($HPBW$). We computed the integrated flux density F by the formula: $F = k_{\rm eff} \times k_i \times T_a/k_{\rm DN}$, where $k_{\rm eff}$ is the factor that takes into account the effective area of the antenna; k_i, the correcting factor that takes into account the differences between the calibrations and the small deviation of the effective area of the antenna during different observing runs; i, the number of the observing run, and $k_{\rm DN}$, the beam pattern factor.

We determined the correcting factor k_i by the sources with known spectra. Depending on the observing year, k_i varied from 1.1 to 1.5. The $k_{\rm eff}$ factor was equal to 3.5.

The power-beam factor $k_{\rm DN}$ indicates how the response from the source weakens with the distance from the central cross section of the power-beam pattern. We computed it for each radio source by the algorithms described by Majorova [15] taking into account the transversal offset of the primary feed along the focal line of the secondary mirror and the vertical distance from the radio source to the central cross section.

As the fidelity criterion we required that the object should be present in scans obtained in at least two observing sets. We computed the mean F and RA values averaged over all observing sets and the corresponding errors.

To build the spectra of the radio sources we used our measured 3.94 GHz flux densities and the data from CATS [16, 17] and VizieR [18] databases that cover the sky area studied, and the data from NED database. We also used the flux densities estimated from the maps of VLSSr (74 MHz) [19, 20], GB6 (4.85 GHz) [21], GLEAM (in the 70–230 MHz frequency interval) [22, 23], and TGSS (150 MHz) [24] surveys. They were obtained for the objects of our list that are absent in the VLSSr, GLEAM, TGSS, and GB6 catalogs, i.e., they are weaker than the detection threshold for reliable sources. We used Aladin tool to estimate fluxes from survey maps.

An analysis of TGSS maps whose angular resolution is better than that of NVSS allowed us to refine the morphology of several radio sources.

We used `spg` software suite [25] to obtain the approximating spectral curves for the sources of the list and compute the spectral indices $\alpha_{3.94}$ and $\alpha_{0.5}$ at 3.94 and 0.5 GHz, respectively, as well as the expected integrated fluxes at 3.94 GHz, which we used to estimate the flux densities of detected sources.

3. CATALOG OF RADIO SOURCES DETECTED AT 7.6 CM IN THE RIGHT-ASCENSION INTERVAL $2^h \leq RA < 7^h$

We detected a total of 237 sources in the right-ascension interval $2^h \leq RA < 7^h$ including 21 blends, 8 double sources resolved in the NVSS survey, and 2 more sources with more than two NVSS components. For several sources 7.7 and 11.1 GHz RATAN-600 measurements were obtained during the same observing runs, and we used them together with other data when reconstructing the spectra of the sources.

The catalog has about 2 min wide gaps at the beginning of each hour when the radiometer was calibrated.

For 124 (52%) sources the fluxes were known at two frequencies, 3.94 GHz (RATAN-600) and 1.4 GHz (VLA), and only 29 such sources (12%)

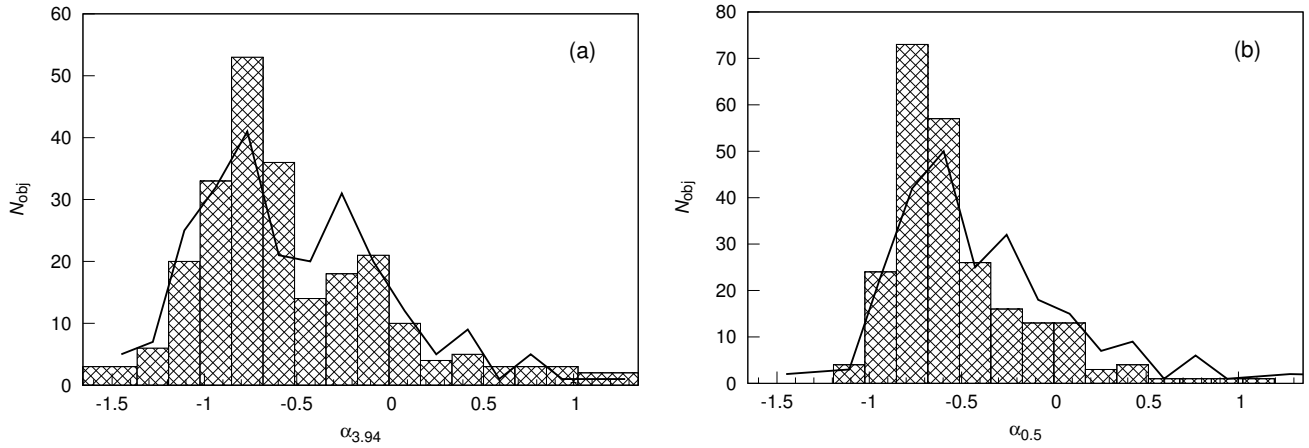

Fig. 1. Distribution of spectral indices for all RCR sources detected in the right-ascension interval $2^h \leq RA < 7^h$: (a) at 3.94 GHz ($\alpha_{3.94}$) and (b) at 0.5 GHz ($\alpha_{0.5}$). The bar graph and the line show the indices determined from spectra obtained with and without using GLEAM and TGSS survey data, respectively.

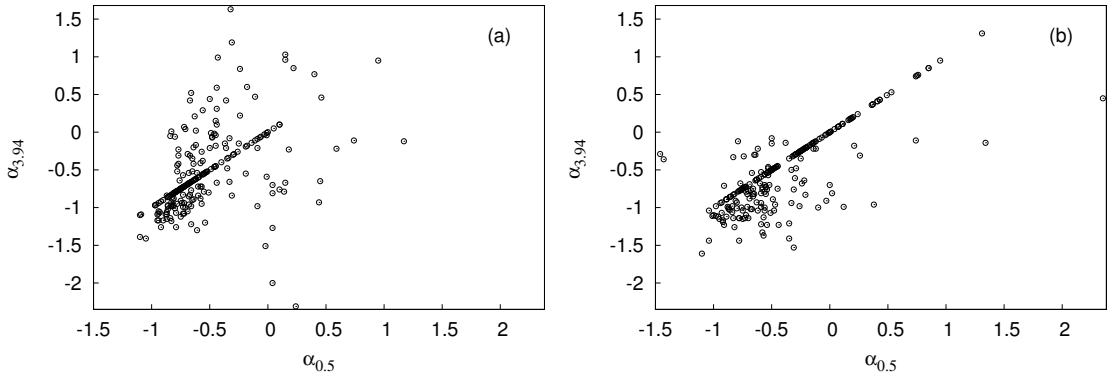

Fig. 2. Distribution of spectral indices at 0.5 and 3.94 GHz for the entire list of sources considered: (a) computed without using the data of the GLEAM and TGSS surveys and (b) computed with GLEAM and TGSS data.

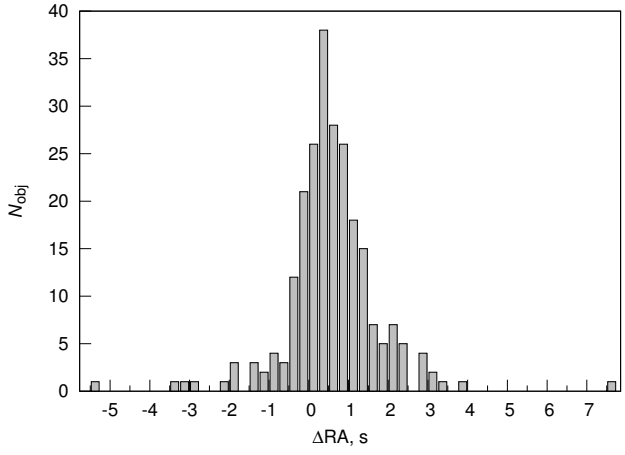

Fig. 3. Distribution of right ascensions $\Delta RA = RA_{NVSS} - RA$ for all RCR sources detected in the right-ascension interval $2^h \leq RA < 7^h$.

remained after the publication of the GLEAM and TGSS catalogs with measurements in the 76–230 MHz frequency interval.

The antenna temperatures of 58 (24%) sources determined from the scans are in the interval $2\sigma \leq T_a < 5\sigma$, where σ is the root-mean-squared noise error in averaged records.

We present the catalog of radio sources detected at 7.6 cm (3.94 GHz) in the right-ascension interval $2^h \leq RA < 7^h$ in Table 1. Column 1[1] gives the coordinates RA_{2000} and Dec_{2000} of the source according to NVSS catalog; column (2) gives the observed right ascension RA transformed to the epoch of 2000.0 and the corresponding measurement error. Column (3) gives the difference of right ascensions, $\Delta RA = RA_{NVSS} - RA$, where RA_{NVSS} is the right

[1]The coordinates of the brightest NVSS source are given for blends and double sources.

ascension of the source according to NVSS catalog. Column (4) gives the integrated flux density F of the source at 3.94 GHz in mJy (averaged over all observing runs) and the corresponding measurement error. Columns (5) and (6) give the spectral indices $\alpha_{3.94}$ and $\alpha_{0.5}$ ($F_\nu \propto \nu^\alpha$) determined at the frequencies of 3.94 and 0.5 GHz, respectively. We chose the latter frequency by analogy with the study by Miley and de Breuck [26].

Table 1. Catalog of 7.6-cm radio sources in the right-ascension interval $2^h \leq RA < 7^h$

RA_{2000} Dec_{2000} NVSS	$RA^{obs}_{2000} \pm \sigma$, hh:mm:ss.ss ± s.ss	ΔRA, s.ss	$F \pm \sigma$, mJy	$\alpha_{3.94}$	$\alpha_{0.5}$	Comments			
(1)	(2)	(3)	(4)	(5)	(6)	(7)	(8)	(9)	(10)
020638.77+044807.2	02:06:35.67	3.10	43.8	-0.73	-0.73	D			
020651.70+044828.6	02:06:49.63±1.76	2.07	31.5 ± 6.0	-0.09	-0.09				
020704.61+050110.4	02:07:04.45±0.27	0.16	10.0 ± 2.0	-1.30	-0.61				
020801.88+050033.3	02:08:01.68±0.36	0.20	18.3 ± 7.5	0.10	0.10		**		#*
020912.54+050051.7	02:09:12.30±0.11	0.24	32.3 ± 2.3	-1.14	-0.84				
020921.70+050142.7	02:09:21.57±0.13	0.13	17.4 ± 3.0	-0.98	-0.83	D			
020931.16+045535.0	02:09:30.18±0.46	0.98	16.1 ± 2.0	-0.75	-0.75	D			
021336.47+051819.2	02:13:33.55	2.92	134.2 ± 3.0	-0.86	-0.86	D			
021449.84+050409.7	02:14:49.42±0.30	0.42	31.6 ± 3.0	-0.72	-0.72	D	**		
021906.86+050354.1	02:19:06.15±0.33	0.71	14.5 ± 1.5	-0.46	-0.46		**		
022019.20+045226.1	02:20:17.07±1.05	2.13	32.3 ± 3.5	-0.02	-0.46		**,vF		
022032.66+050243.6	02:20:32.37±0.14	0.29	60.7 ± 4.0	-0.94	-0.72				
022046.45+050439.2	02:20:45.86±0.3	0.59	15.6 ± 5.0	-1.27	0.04		**	MPS	*
022141.42+044349.3	02:21:38.30±0.88	3.12	151.0 ± 62.0	-1.07	-0.79	D			*
022218.69+050343.8	02:22:19.22±0.18	-1.22	26.8	-1.14	-0.90	b			
022419.41+045657.3	02:24:18.81±0.49	0.60	19.0 ± 3.0	-0.36	-0.36	b			
022509.74+050837.4	02:25:07.63±0.05	2.11	54.0 ± 7.0	-1.17	-0.90				
022528.41+045316.2	02:25:27.65±0.94	0.76	33.7 ± 2.0	-0.95	-0.57				
022619.89+044631.5	02:26:19.31±1.65	0.58	54.0 ± 14.0	-0.94	-0.74	D			*
022653.88+045233.4	02:26:54.17±1.23	-0.29	24.2 ± 4.0	0.05	0.05	2S			
022836.14+045619.2	02:28:35.60±0.87	0.54	17.0 ± 1.0	-0.52	-0.52				
022929.95+045318.0	02:29:28.81±0.63	1.14	29.6 ± 3.0	-1.18	-0.83				
023126.85+045846.4	02:31:27.03±0.33	-0.18	13.8 ± 3.0	-0.85	-0.85	D			
023155.98+050234.4	02:31:55.84±0.32	0.14	18.0 ± 2.0	-0.54	-0.54		**,v?		
023331.40+044909.3	02:33:31.07±1.61	0.33	35.7 ± 7.0	-0.84	-0.84	D			
023407.16+044642.7	02:34:05.47±0.34	1.69	271.0 ± 56.0	-0.22	0.59		**	GPS?	*
023546.15+045111.4	02:35:46.51±0.43	-0.36	27.5 ± 3.5	-0.66	-0.66				
023840.05+045516.8	02:38:39.77±0.34	0.23	48.9 ± 5.0	-0.78	-0.78	b+D			
023950.49+050042.9	02:39:50.38±0.11	0.11	19.6 ± 7.0	-0.69	-0.69		**		*
024309.09+045643.3	02:43:09.09±0.54	0.00	16.3 ± 3.5	-0.55	-0.55				*
024322.22+045804.2	02:43:22.24±0.74	-0.02	12.7 ± 1.0	-0.05	-0.84			upt	
024430.44+044445.8	02:44:29.72±1.70	0.72	59.2 ± 1.0	-0.71	-0.71	D			
024754.12+045414.2	02:47:53.73±0.51	0.39	18.4 ± 3.5	0.31	-0.44			upt	#
024816.44+045345.0	02:48:15.91±0.68	0.53	26.5 ± 12.0	-0.73	-0.73	D			*
024939.93+044028.8	02:49:38.45±3.33	1.48	133.0 ± 22.0	-0.96	-0.68				
025239.26+045840.3	02:52:38.59±0.16	0.67	31.0 ± 2.6	-0.67	-0.44		**,vF		
025253.93+050226.0	02:52:53.80±0.24	0.13	21.8 ± 3.0	-0.62	-0.62	D			
025311.49+050032.2	02:53:11.19±0.40	0.30	10.3 ± 2.5	-0.40	-0.40				#*
025421.04+045723.9	02:54:20.49±0.18	0.55	17.3 ± 2.0	-0.62	-0.62				
025630.94+050221.1	02:56:30.72±0.26	0.22	25.5 ± 2.0	-1.00	-0.71	D			
025647.96+050014.1	02:56:46.65±0.48	1.31	8.5 ± 2.0	-0.68	-0.68				*

Table 1. (Cont.)

RA_{2000} Dec_{2000} NVSS	$RA^{obs}_{2000} \pm \sigma$, hh:mm:ss.ss ± s.ss	ΔRA, s.ss	$F \pm \sigma$, mJy	$\alpha_{3.94}$	$\alpha_{0.5}$	Comments			
(1)	(2)	(3)	(4)	(5)	(6)	(7)	(8)	(9)	(10)
025831.38+045309.0	02:58:30.20±1.66	1.18	29.5 ± 7.0	-0.72	-0.72	D			*
025856.77+050410.4	02:58:55.88±0.17	0.89	18.9 ± 2.0	-0.78	-0.78	D			
030256.65+045521.1	03:02:56.04±0.35	0.61	58.1	-1.05	-0.94	D	vF		
030321.00+050143.5	03:03:20.79±0.46	0.21	14.8 ± 1.0	-0.56	-0.56		vF		
030357.72+050240.7	03:03:56.33±0.66	1.39	12.0 ± 2.0	0.04	-0.71				
030456.91+045640.4	03:04:57.25±0.81	-0.34	12.5 ± 2.0	0.59	-0.44			upt	#
030546.02+045243.3	03:05:44.10±1.25	1.92	26.4 ± 12.0	-0.75	-0.75				*
030626.32+045137.2	03:06:25.48±0.71	0.84	37.8 ± 6.0	-0.78	-0.78	D			
030656.53+045719.3	03:06:56.00±0.14	0.53	53.8 ± 8.0	-0.98	-0.66	D			
030726.37+045517.5	03:07:29.31±1.30	-2.94	15.8 ± 2.0	-0.97	-0.97	D			
030733.90+045304.6	03:07:31.48±1.30	2.42	23.5 ± 2.0	-0.01	-0.49				
030810.14+050226.7	03:08:10.15±0.32	-0.01	12.0 ± 2.0	0.22	-0.24	b	vF		#
030833.98+045409.2	03:08:31.69±0.75	2.29	34.4 ± 2.0	-0.64	-0.64		**,vF		
031114.39+050314.6	03:11:14.48±0.30	-0.09	26.3 ± 2.0	-0.81	-0.81	D			
031124.23+050742.7	03:11:24.59	-0.36	29.2	-0.59	-0.59	D			
031147.96+050802.4	03:11:46.51±0.31	1.45	100.1 ± 16.0	-1.41	-1.05	D	vF		
031321.84+050452.1	03:13:21.33±0.41	0.51	16.9 ± 4.0	-0.97	-0.97	D			*
031347.01+044724.5	03:13:43.70±3.40	3.31	45.1 ± 4.0	0.96	0.15			upt	
031532.21+050721.0	03:15:29.78±1.00	0.22	40.4 ± 6.5	-0.79	-0.79	d			
031705.35+045838.2	03:17:05.42±0.07	-0.07	13.2 ± 1.0	0.15	-0.45				#
031736.52+045545.0	03:17:34.91±0.78	1.61	14.9 ± 2.0	-0.15	-0.25				
031752.52+045452.7	03:17:51.70±0.20	0.82	22.5 ± 4.0	0.47	-0.11			upt	#
031841.77+044137.1	03:18:41.66±0.55	-0.50	188.0 ± 24.0	-1.07	-0.93	b+d	vF		
031844.85+050614.4	03:18:43.38±0.67	1.47	47.9 ± 7.0	-0.80	-0.51		vF		
031858.07+045914.3	03:18:58.10±0.11	-0.03	58.8 ± 5.0	-0.29	-0.69	D	vF	upt	
031903.22+045607.9	03:19:03.71±0.04	-0.49	30.0 ± 5.0	-0.45	-0.45				#
031926.47+050448.7	03:19:25.11±0.42	1.36	96.7 ± 7.5	-0.68	-0.68	D			
032125.00+045849.6	03:21:24.72±0.13	0.28	14.0 ± 3.0	-0.17	-0.62		vF	upt	*
032314.72+044612.7	03:23:13.70±0.71	1.02	143.1 ± 18.0	-0.11	0.74		**,vF	h	
032407.34+044200.2	03:24:07.36±0.46	-0.02	141.5 ± 25.0	-1.08	-0.94				
032456.18+044640.9	03:24:54.53±1.18	1.65	88.1 ± 12.0	-2.00	0.04		vF	MPS	
032506.09+050110.1	03:25:04.33	1.76	14.3	1.19	-0.31				#
032642.23+044650.7	03:26:40.02±0.98	0.98	51.4 ± 8.5	-0.76	-0.76	b+D			
032724.74+045559.6	03:27:23.92±0.43	0.82	11.5 ± 2.0	-0.31	-0.77	D			
032825.57+045344.9	03:28:24.76±0.81	1.24	50.3 ± 6.0	-0.86	-0.86	b+D			
032910.98+050336.5	03:29:10.53±0.22	0.47	26.9 ± 2.0	-0.51	-0.74	b		h	
032917.08+050443.6	03:29:17.12±0.10	-0.04	13.6 ± 3.0	-0.79	-0.79	D			*
032935.83+045549.0	03:29:35.58±1.17	0.25	11.6 ± 3.0	0.99	-0.43	2S		upt	#*
033226.75+045718.7	03:32:26.13±0.06	0.62	23.5 ± 5.0	1.63	-0.32		v?	upt	*
033510.40+045723.3	03:35:09.95±0.08	0.45	44.7 ± 2.0	-0.98	-0.09		**,vF	MPS	
033524.20+050038.3	03:35:23.87±0.11	0.33	11.5 ± 2.0	0.29	-0.56				#
033613.25+045935.9	03:36:12.68±0.22	0.57	8.9 ± 2.0	-0.72	-0.72				*
033726.67+045005.5	03:37:25.71±0.66	0.29	87.3 ± 11.0	-0.99	-0.78	b	**,vF		
033750.84+045833.2	03:37:50.84±0.84	0.00	12.1 ± 1.0	-0.77	-0.77	D	vF		
033901.60+051542.4	03:38:59.11±0.21	2.49	70.0 ± 7.0	-0.79	-0.79	D			
033959.59+050058.3	03:39:58.82±0.18	0.77	12.8 ± 2.0	-0.01	-0.01		vF		#
034024.79+045829.8	03:40:24.72±0.23	0.07	22.0 ± 2.0	-0.59	-0.01		**,vF	MPS	

Table 1. (Cont.)

RA_{2000} Dec_{2000} NVSS	$RA^{obs}_{2000} \pm \sigma$, hh:mm:ss.ss ± s.ss	ΔRA, s.ss	$F \pm \sigma$, mJy	$\alpha_{3.94}$	$\alpha_{0.5}$	Comments			
(1)	(2)	(3)	(4)	(5)	(6)	(7)	(8)	(9)	(10)
034041.76+045736.3	03:40:41.52±0.73	-0.52	13.5 ± 5.0	-0.04	-0.45	b			*
034109.80+050709.6	03:41:08.94±0.61	0.86	56.9 ± 7.0	-0.97	-0.86	D			
034151.93+045925.3	03:41:53.94±3.03	-2.01	9.0 ± 1.0	-0.34	-0.34				
034231.79+044740.6	03:42:29.63±1.62	2.16	70.8 ± 2.0	-0.72	-0.60		vF		
034243.15+044527.5	03:42:43.33	-0.18	82.6	-0.68	-0.68	D			
034329.99+045750.3	03:43:29.78±0.23	0.21	1133.1	-0.97	-0.83	D	v		
034554.43+045729.5	03:45:54.87±0.70	-0.44	15.3 ± 1.0	-0.75	-0.75	D			
034628.75+045545.5	03:46:28.03±0.76	-0.03	17.3	-0.06	-0.80	d			
034656.76+045653.8	03:46:56.86±0.01	-0.10	12.3 ± 3.0	-0.21	-0.36				*
034824.81+045421.7	03:48:23.99±0.54	0.82	24.3 ± 3.0	-0.46	-0.46		vF		
034828.10+050151.6	03:48:27.07	1.03	12.3 ± 2.0	-0.42	-0.77				
034901.48+051038.4	03:49:01.36±0.69	0.12	66.1 ± 10.0	-0.76	-0.76				
034931.08+050042.4	03:49:31.17±0.33	-0.09	25.0 ± 1.0	-0.67	-0.67	D			
034940.30+045731.2	03:49:40.27±0.36	0.03	15.8 ± 4.0	-0.04	-0.01		vF		#*
035054.23+050620.9	03:50:52.59±0.28	0.41	399.4 ± 27.0	-0.67	0.15	b		MPS	
035203.68+044612.0	03:52:05.06±0.74	-1.38	59.9 ± 8.0	-0.84	-0.31				
035208.14+045128.5	03:52:05.22	2.92	35.6 ± 5.0	-0.83	-0.83				
035303.88+050431.1	03:53:01.74±0.33	2.14	32.5 ± 1.5	-0.15	-0.37				
035424.14+044107.3	03:54:23.61±1.04	0.53	190.4 ± 8.0	-0.07	-0.07			h	
035454.40+050250.2	03:54:54.81	-0.41	21.1	-0.97	-0.81				
035515.52+045703.1	03:55:14.37±0.56	1.15	9.2 ± 2.0	0.84	-0.24		**	upt	#*
035602.18+045602.8	03:56:01.30	0.88	15.8	-0.76	-0.76				
035659.95+045947.7	03:57:00.77±0.21	-0.82	9.1 ± 1.5	-0.29	-0.29				#
035815.51+045449.1	03:58:13.20±0.05	2.31	12.5 ± 4.0	0.42	-0.36				#*
040311.59+045929.0	04:03:11.22±0.93	0.37	8.2 ± 3.0	0.10	0.10				#*
040332.04+045817.3	04:03:31.62±0.22	0.42	45.8 ± 6.0	-0.79	0.14			MPS	
040404.37+045839.5	04:04:03.80	0.57	10.4 ± 2.0	-0.55	-0.55		**		
040424.21+050633.6	04:04:26.29±0.03	-1.29	43.6 ± 2.0	-0.82	-0.82	b			
040427.26+050207.2	04:04:26.29	0.97	39.4 ± 2.0	-0.79	-0.79				
040626.84+044753.2	04:06:28.66±4.50	-1.82	61.4 ± 10.0	-0.92	-0.92				
041034.32+045540.3	04:10:33.13±0.61	1.19	12.6 ± 4.0	-0.08	-0.33				*
041319.72+045839.7	04:13:19.54±0.17	0.18	25.2 ± 3.0	-0.42	-0.64				
041330.97+045247.7	04:13:32.18±0.67	-1.21	31.7 ± 3.0	-0.60	-0.60				
041510.24+050144.4	04:15:08.92±0.56	1.32	10.9 ± 4.0	-0.64	-0.76				*
041752.68+044404.8	04:18:01.30	-5.30	66.7 ± 15.0	-0.35	-0.65	b			*
042003.08+045101.9	04:20:02.54±0.29	0.54	41.8 ± 6.0	-0.45	-0.45				
042154.98+050230.5	04:21:54.72±0.23	0.26	17.8 ± 2.0	-0.18	-0.45		**		
042333.58+045451.3	04:23:32.37±0.32	1.21	20.1 ± 5.0	-0.69	-0.69				
042545.15+045028.3	04:25:43.85±2.50	1.30	24.9 ± 3.0	-0.49	-0.49				
042619.18+045025.7	04:26:18.78±0.40	0.40	434.4 ± 54.0	-1.12	-0.75				
042636.60+051818.0	04:26:29.00	7.60	375.0	-0.23	0.18			MPS	
042747.61+045708.9	04:27:47.15±0.20	0.46	642.7 ± 73.0	-0.26	-0.26		v		
043311.04+052115.4	04:33:10.17±1.65	0.83	1878.0 ± 200.0	-0.21	-0.09	mc	v	h	
043551.33+045612.6	04:35:49.90	1.43	10.4 ± 3.0	-0.86	-0.86				*
043558.30+045723.9	04:35:57.64	1.36	9.2 ± 2.0	-0.06	-0.06	b(d?)			#*
043611.99+050127.0	04:36:11.68±0.38	0.31	13.3 ± 2.0	-0.66	-0.66				
043629.74+050034.9	04:36:29.56±0.56	0.18	16.2 ± 3.0	-0.30	-0.30				

Table 1. (Cont.)

RA_{2000} Dec_{2000} NVSS	$RA^{obs}_{2000} \pm \sigma$, hh:mm:ss.ss ± s.ss	ΔRA, s.ss	$F \pm \sigma$, mJy	$\alpha_{3.94}$	$\alpha_{0.5}$	Comments			
(1)	(2)	(3)	(4)	(5)	(6)	(7)	(8)	(9)	(10)
043722.65+050529.6	04:37:26.03±1.38	-3.38	25.0 ± 3.0	-0.64	-0.64				
043732.83+045139.0	04:37:29.06	3.77	11.0 ± 3.0	-1.39	-1.10				*
043848.16+044936.2	04:38:48.37±0.74	-0.21	46.3 ± 15.0	-0.57	-0.73				*
044014.54+050002.9	04:40:13.42±0.17	1.12	15.3 ± 1.0	0.01	-0.83			upt	
044136.20+045403.4	04:41:35.08±0.05	1.12	19.9 ± 5.0	-0.70	0.04			MPS	#*
044148.48+044848.7	04:41:51.62	-3.14	28.3 ± 3.0	-0.38	-0.56				
044417.89+050126.8	04:44:17.57±0.18	0.32	64.6 ± 5.0	-1.09	-0.95	D			
044455.22+045659.7	04:44:55.27±0.61	-0.05	22.0 ± 7.0	0.85	0.22				#*
044924.30+045844.5	04:49:58.86±0.23	0.89	11.7 ± 2.0	-1.08	-0.73				
044935.43+050102.3	04:49:33.81±0.15	1.62	11.9 ± 2.0	-0.54	-0.61				
045000.72+051254.9	04:49:58.86	2.14	33.2 ± 5.0	-0.62	-0.62	b			
045110.15+045054.8	04:51:10.07±0.57	0.08	38.3 ± 14.0	-0.72	-0.57	d			*
045113.48+043751.2	04:51:11.11	2.37	30.6	-0.88	-0.58		**		
045151.26+050134.7	04:51:49.65	1.61	9.1 ± 3.0	-0.74	-0.74				*
045322.45+051052.6	04:53:22.78	-0.33	57.2 ± 8.0	-0.12	1.17		**	GPS	
045503.78+045302.0	04:55:03.22±0.35	0.56	35.3 ± 7.0	-1.06	-0.93				
045544.48+045051.9	04:55:43.22±0.54	1.26	32.8 ± 4.0	-0.53	-0.53				
045754.69+045354.3	04:57:53.76±0.28	0.93	75.7 ± 7.5	-0.98	-0.86				
045815.27+050410.4	04:58:14.84±0.38	0.43	71.3 ± 7.0	-1.17	-0.94				
045905.59+045609.8	04:59:05.18±0.24	-0.18	99.8 ± 8.0	-0.91	-0.81	d+b			
050523.20+045942.8	05:05:22.69±0.12	0.51	1000.0 ± 63.0	-0.11	-0.11		v	h	
050625.10+050819.7	05:06:23.08±0.59	2.02	66.4 ± 6.0	-0.83	-0.67		v?		
050649.14+045101.7	05:06:48.74±1.33	0.40	29.6 ± 9.0	0.02	-0.62				*
050709.01+045520.0	05:07:08.68±0.01	0.33	33.8 ± 3.0	-0.88	-0.81				
050825.45+045155.4	05:08:24.63	0.82	29.6	-0.90	-0.90				
051006.04+045910.0	05:10:04.86±0.30	1.18	11.7 ± 2.0	-0.21	-0.50				
051018.00+045952.7	05:10:18.47±2.25	-0.47	12.9 ± 1.0	-0.14	-0.14				#
051106.30+045854.5	05:11:05.75±0.34	0.55	15.2 ± 1.0	-0.76	-0.76				
051219.39+045610.8	05:12:18.90±0.83	0.49	17.5 ± 2.0	0.10	-0.44				
051343.45+045854.7	05:13:43.15±0.09	-0.85	33.8 ± 5.0	-1.51	-0.02	b	v?	MPS	
051359.03+050235.7	05:13:59.14±0.48	-0.11	22.0 ± 2.0	-0.65	0.45			GPS	#
051539.19+045947.5	05:15:38.93±0.43	0.26	9.0 ± 1.0	-0.35	-0.35				
051711.68+050032.6	05:17:11.40±0.13	0.28	44.0 ± 4.0	-0.18	-0.18		**	h	
051909.69+050520.3	05:19:09.20±0.26	0.49	31.0 ± 7.0	-0.69	-0.69				*
052035.50+045401.7	05:20:34.68±0.38	0.82	33.0 ± 4.0	-0.52	-0.78		**	h	
052055.49+050654.7	05:20:53.72±0.75	1.77	46.0 ± 4.0	-0.95	-0.78				
052117.03+050728.8	05:21:17.39±0.67	-0.36	80.0 ± 12.0	-0.93	0.44			GPS	
052241.76+045304.3	05:22:41.85±1.10	-0.09	21.0 ± 5.0	-0.31	-0.67				*
052326.80+045918.6	05:23:26.30±0.25	0.50	16.0 ± 3.0	-0.76	0.10			GPS	#
052331.28+050844.2	05:23:30.13±0.81	1.15	66.0 ± 24.0	-1.06	-0.87				*
052333.28+045827.7	05:23:32.44	0.84	19.0 ± 5.0	-0.84	-0.60				*
052431.59+050736.6	05:24:30.50±1.00	1.09	39.0 ± 5.0	-0.81	-0.81				
052502.08+045432.7	05:25:01.38±0.26	0.70	85.0 ± 9.0	-0.83	-0.73				
052719.63+050153.9	05:27:17.70±0.25	1.93	41.0 ± 3.0	-0.89	-0.64				
052801.46+045750.1	05:28:01.14±0.06	0.32	46.0 ± 1.0	-0.56	-0.56				
053207.80+050243.6	05:32:06.69±0.30	0.31	18.0 ± 3.0	-0.70	-0.70	d			
053435.41+050342.5	05:34:34.69±0.23	0.72	240.0 ± 21.0	-1.09	-0.87				

Table 1. (Cont.)

RA_{2000} Dec_{2000} NVSS	$RA^{obs}_{2000} \pm \sigma$, hh:mm:ss.ss ± s.ss	ΔRA, s.ss	$F \pm \sigma$, mJy	$\alpha_{3.94}$	$\alpha_{0.5}$	Comments			
(1)	(2)	(3)	(4)	(5)	(6)	(7)	(8)	(9)	(10)
053603.93+050600.6	05:36:02.47±0.95	1.46	29.0 ± 5.0	-0.94	-0.94				
053816.21+045239.5	05:38:13.30±0.45	2.91	27.0 ± 4.0	-0.41	-0.58				
053849.53+050411.5	05:38:50.66±0.48	-0.66	30.0 ± 4.0	-0.81	-0.81	d			
053957.88+045359.5	05:39:57.08±0.33	0.80	33.0 ± 5.0	-0.81	-0.81				
054118.70+050900.2	05:41:16.93±0.45	1.77	100.0 ± 20.0	-1.02	-0.86				*
054246.21+045419.6	05:42:45.70±0.18	0.51	58.0 ± 5.0	-0.55	-0.19		**	MPS	
054405.13+045906.4	05:44:03.47±0.34	1.66	14.0 ± 1.0	-0.20	-0.64				
054555.90+045943.6	05:45:55.15	0.75	12.0	-0.63	-0.63		**		
054948.75+045246.4	05:49:47.66±1.00	1.09	32.0 ± 9.0	-0.52	-0.65				*
055256.16+044725.3	05:52:53.17±0.48	2.99	94.0 ± 2.0	-1.08	-0.72	d?			
055313.77+045549.6	05:53:13.33±0.31	0.44	42.0 ± 5.0	-2.31	0.24		**	MPS	
055652.59+050937.2	05:56:51.44±1.50	1.15	46.0 ± 6.0	-1.20	-0.54			MPS	
055902.37+045304.8	05:59:01.54±1.40	0.83	28.0 ± 2.0	-0.77	-0.66				
055936.84+045800.8	05:59:36.58±0.02	0.26	16.0 ± 2.0	-1.17	-0.95				
060404.70+045657.4	06:04:04.92	-0.92	12.0 ± 2.5	-0.87	-0.32	d			#*
060428.72+045958.8	06:04:28.14±0.77	0.58	12.0 ± 3.0	-0.68	-0.68				*
060537.91+050020.5	06:05:39.40±0.35	-1.49	11.0	0.42	-0.67			upt	
060612.31+045743.1	06:06:12.10±0.40	0.21	22.0 ± 3.0	-0.53	-0.53		**,v?		
060659.73+050659.2	06:06:58.30±0.40	1.43	46.0 ± 9.0	-0.85	-0.68		v?		
060715.71+045818.9	06:07:16.24±0.33	-0.53	9.0 ± 3.0	-0.74	-0.74				*
060829.14+050115.3	06:08:28.16±0.16	0.98	15.0 ± 4.5	-0.75	-0.50	d?			*
060947.02+045927.9	06:09:47.00±0.22	0.02	11.0 ± 2.0	-1.26	-0.92				
061003.66+045354.1	06:10:03.11	0.55	14.0 ± 3.0	-0.84	-0.87		v?		*
061028.84+050025.8	06:10:28.51±0.43	0.33	16.0 ± 2.0	-0.91	-0.75				
061048.06+050504.4	06:10:47.88	0.18	15.0 ± 3.0	-0.23	-0.77				
061217.47+045636.7	06:12:17.20±0.10	0.27	16.0 ± 7.0	1.03	0.15				#*
061553.63+045650.9	06:15:52.98±0.90	0.65	13.0 ± 4.0	-1.26	-0.79				
061627.92+045312.0	06:16:26.48±0.50	1.44	15.0 ± 3.0	-0.06	-0.48				
061756.20+045824.9	06:17:56.61	-0.41	7.0 ± 3.0	0.60	-0.18			upt	#*
061823.59+050700.1	06:18:21.87	1.72	33.0 ± 7.0	-0.07	-0.48				*
061900.21+050630.8	06:18:59.30±0.13	0.91	299.0 ± 27.0	-0.81	0.04	b	v?	MPS	
061909.63+045400.1	06:19:08.87±0.37	0.76	47.0 ± 1.0	0.52	-0.66	b		upt	
061943.49+045748.3	06:19:42.86	0.63	12.0 ± 5.0	-0.80	-0.80				*
062130.07+045258.2	06:21:28.74±0.22	1.33	37.0 ± 5.0	-0.72	-0.58	b	**		
062152.90+043834.4	06:21:51.84±1.00	1.06	392.0 ± 33.0	-1.01	-0.80				
062157.68+045606.8	06:21:57.37±0.14	0.31	61.0 ± 11.0	-0.79	-0.55		**		
062207.41+045651.1	06:22:07.48±0.15	-0.07	25.0 ± 4.0	-0.90	-0.65		v?		
062310.75+050410.0	06:23:11.86±0.14	-1.86	65.0 ± 11.0	-0.74	-0.74	D+D	v?		
062325.66+045624.1	06:23:25.32±0.25	0.34	12.0 ± 2.0	-0.19	-0.19				#
062418.85+045701.8	06:24:18.37±0.23	0.48	165.0 ± 30.0	-0.99	-0.73				
062450.96+050350.0	06:24:50.61±0.38	0.35	22.0 ± 4.0	-1.05	-0.69				
062549.27+045648.2	06:25:48.46±0.30	0.81	28.0 ± 9.0	0.44	-0.50			upt	*
062741.83+045803.9	06:27:41.55	0.28	52.0	-0.98	-0.82		**,v?		
063759.26+045505.5	06:37:59.04±0.67	0.22	18.0 ± 2.0	0.77	0.40				#
063826.31+045246.6	06:38:26.44±0.94	-0.13	27.0 ± 4.5	-0.79	-0.79				
063929.62+045937.0	06:39:29.64±0.27	-0.02	17.0 ± 4.0	-0.26	-0.57		**,v?		*
064054.67+050550.3	06:40:54.00±0.01	0.67	36.0 ± 4.0	-0.44	-0.78				

Table 1. (Cont.)

RA_{2000} Dec_{2000} NVSS	$RA^{obs}_{2000} \pm \sigma$, hh:mm:ss.ss ± s.ss	ΔRA, s.ss	$F \pm \sigma$, mJy	$\alpha_{3.94}$	$\alpha_{0.5}$	Comments			
(1)	(2)	(3)	(4)	(5)	(6)	(7)	(8)	(9)	(10)
064116.31+044748.5	06:41:15.32±0.71	0.99	59.0 ± 18.0	-1.22	-0.66				*
064415.38+050641.5	06:44:14.15±0.40	1.23	119.0 ± 5.0	-0.93	-0.83				
064753.44+050456.5	06:47:53.66±0.13	-0.22	24.0 ± 3.0	0.95	0.95				#
065110.86+045356.1	06:51:10.86	0.00	17.0 ± 6.0	0.21	-0.63				*
065327.47+050851.6	06:53:26.76±0.46	0.24	149.0 ± 16.0	-0.48	-0.35	b	**		
065529.90+045510.9	06:55:29.61±0.23	0.29	48.0 ± 6.0	-0.03	-0.03		**		
065850.15+050206.7	06:58:49.05±0.71	1.10	40.0 ± 7.0	0.00	0.00		v?		
065929.43+045603.8	06:59:30.37±0.92	-0.94	13.0 ± 2.0	0.46	0.46		v?		#

In column (7) we mark double sources and blends:

D—the object is a double source in the FIRST or TGSS survey, which is not resolved by the RATAN-600 power-beam pattern;
2S—the object consists of two unassociated FIRST or TGSS sources, which are not resolved in NVSS;
d—objects which are resolved into two components in the NVSS survey and hence also in the "Cold" surveys;
t—the sources with three or more (mc) NVSS components.
b—blends with further clarification:
b(d?)—two sources or, possibly, a double source unresolved by the power-beam pattern of RATAN-600;
b+d—a point source blended with a double source;
b+D—a point source blended with a double FIRST source.

Column (8) marks specific features of flux density variations, namely:

**—large scatter of flux data at different frequencies;
v—object is known to be variable according to published studies;
v?—sources suspected to be variable by Majorova et al. [27];
vF—the flux reported in the FIRST survey is greater than in NVSS, which may be indicative of possible variability.

Column (9) serves to mark the specific features of the radio spectrum:

h—spectra ("hill") made up of a power-law spectrum superimposed onto a spectrum with self-absorption at frequencies from 0.5 to 12 GHz;
GPS (Giga Hertz Peak Spectrum) or MPS (Mega Hertz Peak Spectrum)—indicates that the radio spectrum has a peak in the GHz or MHz frequency range, respectively;
upt ("upturn")—indicates that the spectrum increases at high frequencies.

The # symbol in column (10) indicates the objects with flux data available only at 1.4 and 3.94 GHz; the * symbol indicates objects whose antenna temperatures in the records fall within the $2\sigma < T_a \leq 5\sigma$ interval.

4. RADIO SPECTRA OF THE SOURCES

We constructed the spectra of the radio sources of our list using the data from VLSSr, TXS [28], NVSS, and GB6 surveys, the new GLEAM and TGSS surveys, and also the data from VizieR, CATS, and NED databases.

Let us now provide some information about the radio surveys used.

VLA Low-frequency Sky Survey (VLSS) was carried out at 74 MHz in 2001–2007 and covers 95% of the sky. The data of this survey were rereduced using a new model of ionospheric distortion and power-beam correction [20]. Based on the results of this reduction a new catalog, VLSSr, was published, which includes about 93 thousand sources and radio maps. The angular resolution of VLSSr and root-mean-square noise error of radio maps are equal to 75″ and 100 mJy, respectively. The detection threshold of VLSSr is of about 500 mJy and strip of the "Cold" surveys is located completely inside the coverage area of VLSS.

GLEAM (GaLactic and Extragalactic All-sky Murchison wide field array survey) covers the southern sky up to the declination of +20° (its coverage area is 7.5 sr). It was carried out in 2013–2014 at 20 frequencies in the 72–231 MHz range with a resolution of about 2′. The catalog contains about 300 thousand sources found at the detection limit 50 mJy. When constructing the spectra of the sources investigated in this study we used the integrated flux densities at all 20 frequencies of the GLEAM survey. No GLEAM data are available for the part of our survey located in the right-ascension interval $5^h45^m < RA < 7^h30^m$.

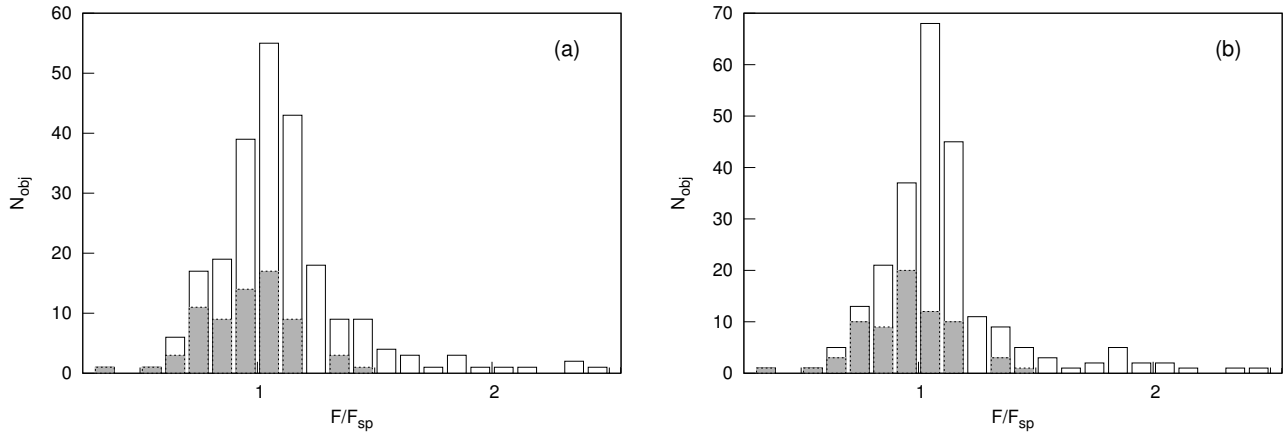

Fig. 4. Distribution of the ratio of the measured flux density F to the flux density F_{sp} expected from the spectrum for the entire sample (empty bars) and for sources with reliably determined fluxes (the gray bars) for the expected fluxes determined from spectra computed (a) with the use of GLEAM and TGSS survey data, (b) without using GLEAM and TGSS data.

TGSS (Tata institute for fundamental research GMRT Sky Survey) is carried out at the Indian Giant Metrewave Radio Telescope (GMRT) at the frequency of 150 MHz. The first alternative TGSS data release ADR1 (Alternative Data Release) [24] was based on observations carried out in 2010–2012 within the framework of this project. The survey covers a sky area of 36 900 □°. It covers 90% of the entire sky from −53° to +90° in declination. For most of the maps the background noise of the power-beam pattern is equal to 5 mJy and the angular resolution is 25″, which is almost twice better than that of NVSS. The catalog includes 620 thousand sources found at the 7σ detection limit. The coordinate and flux density accuracy is equal to 2″ and 10%, respectively. The rather high angular resolution of TGSS made it possible to refine the morphological structure of some of the sources studied, for which no FIRST maps were available.

The GB6 (Green Bank 4.85 GHz, $\lambda \sim 6$ cm) survey was carried out at the NRAO 91-m telescope in 1986–1987. It covers the sky from 0° to +75° in declination, includes 75 thousand sources brighter than 18 mJy [21].

4.1. Flux Density Estimates for RCR Sources Based on Survey Radio Maps

Before the publication of GLEAM and TGSS surveys, which at low frequencies are more sensitive than VLSSr and TXS, integrated flux densities for almost one half of the sources were known only at two frequencies – 1.4 and 3.94 GHz – i.e., sustainable spectral fitting could be performed only for the other half of the objects. For this reason for all sources with no available flux densities in the GB6 and VLSSr catalogs we estimated their fluxes from the maps of the corresponding surveys. We estimated the integrated flux densities for the sources with appreciable excess of signal above the visually estimated background level at their locations. To this end, we compared the aperture magnitudes[2] of the catalogued object and the sources studied. For the sources with no excess above the background detected during observations we set a limit of about 1σ, i.e., 100 and 5 mJy for VLSSr and GB6, respectively. When fitting the radio spectra we set the weight factors for such estimates at 5–30% of the weight factors for catalogued flux densities.

After the publication of the GLEAM and TGSS surveys a total of 12% of all sources remained with flux data available only at two frequencies. In most of the cases GLEAM and TGSS catalog data confirmed the flux estimates based on VLSSr maps in locations with excess above the background level.

The flux density estimates based on GLEAM and TGSS maps were also made for a number of sources, as it was done for VLSSr and GB6 maps. For sources with no signal excess above the background level we set the limit at 1σ, i.e., 10 and 5 mJy for GLEAM and TGSS, respectively.

4.2. Spectral Indices of RCR Sources

To construct the radio spectra we fitted the quantities by a first or second-order polynomial.

[2]We used the corresponding function of Aladin application to compute the integrated magnitudes in the given aperture.

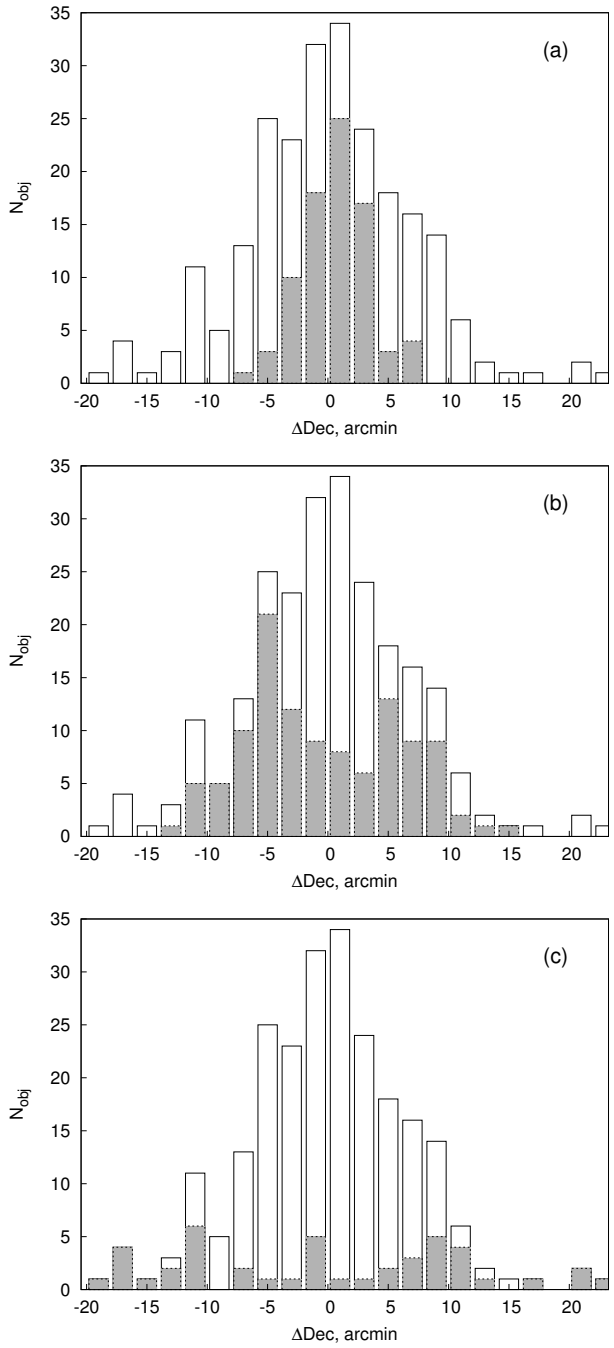

Fig. 5. Comparison of the deviations ΔDec from the central cross section of the "Cold" surveys for the entire list of sources (the empty bars) and for flux-limited samples (the gray bars): (a) $F_{3.94\,GHz} \leq 17.5$ mJy, (b) $17.5 < F_{3.94\,GHz} \leq 60$ mJy, (c) $F_{3.94\,GHz} > 60$ mJy.

We now show the distribution of spectral indices for the list studied at 3.94 and 0.5 GHz (Fig. 1) comparing how the indices changed after incorporating GLEAM and TGSS data.

The histogram of spectral indices $\alpha_{3.94}$ (Fig. 1a, the line) shows well-defined maxima at -0.8 and -0.3 and not very distinct maximum at $+0.45$, which coincides with the distribution for sources of RCR catalog [10] in the right-ascension interval $7^{\rm h} \leq {\rm RA} < 17^{\rm h}$. Sources with steep spectra ($\alpha_{3.94} \leq -0.5$) made up for 58% of the sample.

The form of the histogram changed with incorporating GLEAM and TGSS data (the bar chart in Fig. 1a), although it also shows three maxima at -0.8, 0.1, and $+0.45$. The number of sources with steep spectra increased to 65%.

The two maxima at -0.6 and -0.25 can also be seen in the distribution of spectral indices at 0.5 GHz $\alpha_{0.5}$ (the line in Fig. 1b), as well as a not very conspicuous maximum at $+0.45$. Sources with steep spectra ($\alpha_{0.5} \leq -0.5$) made up for 54% of the sample.

After incorporating GLEAM and TGSS data the distribution of spectral indices (the bar diagram in Fig. 1b) at 0.5 GHz shows a well-defined maximum at -0.8 and rather inconspicuous maxima at 0.0 and $+0.45$. The fraction of sources with steep spectra increased to 68%.

Here are the source features marked in Table 1, which hinder reliable determination of indices:

- blending, i.e., sources that cannot be resolved by the RATAN-600 power-beam pattern (21, or 9%), which brings uncertainty to the flux density measurements ("b" in the table);
- scarce data: for 29 (12%) sources fluxes are known only at two frequencies (#);
- large scatter of fluxes at different frequencies, which is observed in 31 sources (13%), spectral indices are determined with errors greater than 50% (**);
- weak signal in the scan—sources (24%) with signal-to-noise ratio no greater than 5 (*);
- variability: flux variations were noted in 40 (18%) sources either from one observing run of "Cold" surveys to another [27] ("v?"), or the flux in the FIRST survey is greater than in the NVSS survey ("vF") with errors taken into account, or variability evidence was published in the literature ("v");
- complex form of spectra, which was found in seven sources (3%) (they are marked by "h" symbol).

The spectral indices for the sources without the above features are determined with an accuracy of about 10%. Before incorporating GLEAM and TGSS data there were 64 (or 27%) such sources and their average and median spectral index were equal to $\overline{\alpha_{3.94}} = -0.83$ and -0.93, respectively, and the average and median spectral index for the entire list are equal to -0.53 and -0.63, respectively. With new low-frequency data incorporated the number of sources with reliably determined spectra increased to 116 (or 49%). Their average and median spectral

index are equal to $\overline{\alpha_{3.94}} = -0.68$ and -0.76, respectively, and the corresponding values for the entire list are -0.55 and -0.68.

4.3. Form of the Spectra of RCR Sources

Here we present plots of the distribution of spectral indices at 0.5 and 3.94 GHz for the entire list of sources, which we determined based on catalogs and our measurements before the publication of GLEAM and TGSS surveys (Fig. 2a) and with GLEAM and TGSS data incorporated (Fig. 2b).

We used flux density estimates made by radio maps of the surveys for 29 (12%) sources with fluxes measured only at two frequencies 1.4 and 3.94 GHz.

As a result, for the entire list studied the spectra of 41% of the sources can be best approximated by a straight line (S spectra). The fraction of sources with such spectra was higher — 51% — when analyzed without using GLEAM and TGSS survey data (Fig. 2a).

About 25% of the sources have steep spectra at 0.5 GHz with the steepness increasing at high frequencies (C^-) (examples of spectra are shown in Fig. 13 in [10]), which is usually interpreted as a result of the loss of energy by high-energy relativistic electrons via radiative cooling. The fraction of sources with C^- spectra was only slightly greater than 29% before incorporating the data from new low-frequency surveys.

In our list 11% of the objects have steep spectra at 0.5 GHz with flattening at higher frequencies (C^+). Examples of spectra can be seen in Fig. 14 in the paper by Soboleva et al. [10]. Such a spectrum can be explained by the superposition of the usual power-law spectrum from extended components of the radio source and the spectrum from features with small angular sizes (ejecta from the nucleus) with self absorption by relativistic electrons at higher frequencies. Without GLEAM and TGSS data C^+-spectra were found in 7% of the sources.

The spectra of 18 (8%) of the sources have a maximum at frequencies 0.5–12 GHz ([10], Fig. 16). Such spectra are observed in CSS (Compact Steep Spectrum), GPS (Gigahertz Peak Spectrum), and HFP (High Frequency Peak) sources. The sources with a maximum in the spectrum are believed to be either young objects or blazars [29–31]. Note that no HFP sources could be found in this list.

Another 7 (3%) sources have spectra with a maximum and a more complex shape (see [10], Fig. 17). It is due to the superposition of the power-law spectrum at low frequencies and self-absorption at 0.5–12 GHz. It is probable that such a spectrum is due to restart of activity at radio frequencies in the active galactic nucleus. Sources with such radio spectra are marked by the "h" symbol ("hill" in [10]).

Sources with a minimum in the spectrum followed by increase at frequencies above 5 GHz (at the top of Fig. 18 in [10]) are called "upturn" in the literature [32]. Such sources make up for 19% of the sample of Tucci et al. [33]. Our list contains three sources with such spectra. After incorporating new data in the 75–230 GHz frequency interval and refining their spectra the number of sources with such spectra increased to 16 (7%).

5. RELIABILITY OF THE IDENTIFICATION OF RCR SOURCES

As the reference catalog for identification and coordinate calibration of RCR sources we used the NVSS catalog because the angular resolution of the corresponding survey is close that of the "Cold" surveys and its better than 1″ coordinate accuracy. We made the decision to identify an RCR source with an NVSS object after visual inspection of the corresponding sky area with Aladin tool superimposing the coordinates of both catalogs onto the $15' \times 15'$ NVSS map. First of all we considered the matching of the right ascensions. To resolve controversial cases involving blending of several sources by the power-beam pattern of RATAN-600 and the cases of weak sources we also used the maps of GB6 survey, whose frequency range is close to that of "Cold" survey, and TGSS survey maps whose resolution is higher than that of NVSS.

5.1. Determination of Right Ascension

Figure 3 shows the distribution of the difference between the observed right ascensions transformed to the epoch of 2000.0 and the right ascensions from NVSS catalog, ΔRA, for 237 sources. The average difference is equal to $\overline{\Delta RA} = 0^s.58 \pm 1^s.18$[3]. The average right-ascension difference for sources with S/N greater than 5 (76% of the sources) is $\overline{\Delta RA} = 0^s.54 \pm 1^s.04$.

We considered the variation of $\overline{\Delta RA}$ in the cases where the source is offset from the central section of three selections: weak ($F \leq 17.5$ mJy), intermediate-brightness ($17.5 < F \leq 60$ mJy), and bright ($F > 60$ mJy) sources. We present the results in Table 2, where column (1) gives the offset range, i.e., "5" corresponds to the source declination ΔDec in the strip from $-5'$ to $+5'$ relative to the central cross

[3]The average difference for sources in the $7^h \leq RA < 17^h$ interval is $\overline{\Delta RA} = 0^s.29 \pm 1^s.08$ [10].

Table 2. Average ΔRA and their errors depending on the offset of sources from the central cross section of the survey ΔDec for the entire list (RCR) and for three flux limited samples

ΔDec	RCR	$F \le 17.5$, mJy	$17.5 < F \le 60$, mJy	$F > 60$, mJy
(1)	(2)	(3)	(4)	(5)
5′	$0^s.37 \pm 0^s.75$	$0^s.35 \pm 0^s.85$	$0^s.41 \pm 0^s.56$	$0^s.38 \pm 0^s.25$
10′	$0^s.73 \pm 1^s.10$	$0^s.88 \pm 1^s.11$	$0^s.73 \pm 1^s.15$	$0^s.61 \pm 0^s.91$
15′	$0^s.65 \pm 2^s.03$	–	$0^s.85 \pm 1^s.75$	$0^s.41 \pm 2^s.30$
20′	$1^s.99 \pm 2^s.11$	–	–	$1^s.99 \pm 2^s.21$

section of the survey, "10"—offset in the interval 5 to 10′ on both sides of the central cross section, etc. Columns (2) to (5) give the $\overline{\Delta RA}$ values and their errors for the entire list considered, for weak, intermediate-brightness, and faint sources.

The $\overline{\Delta RA}$ differences agree well for weak, intermediate-brightness, and bright sources in the case of small offsets $\Delta Dec \le \pm 5'$. For large offsets $|\Delta Dec| > 15'$ the errors of the determination of right ascension of the sources increase and so does the difference between the observed RA and RA_{NVSS}. This is due to both the variation of the form of the power-beam pattern with increasing deviation from the central cross section, and to errors of fitting a Gaussian to the signal on the scan obtained with expanding power-beam pattern.

5.2. Determination of Integrated Flux Density

We compared the integrated flux densities F measured at 3.94 GHz with the expected flux densities F_{sp} computed from the spectra. We initially did it for spectra constructed based on available data from CATS, VizieR, and NED before the publication of low-frequency GLEAM and TGSS surveys, and then incorporating the new information published in these catalogs. For further comparison below we also list the expected integrated fluxes computed from the spectra without using GLEAM and TGSS data. These fluxes are marked as "old."

The mean ratio averaged over the entire list of radio sources is $\overline{F/F_{sp}} = 1.15 \pm 0.48$, and the corresponding median is 1.07; the mean and median ratio computed without using GLEAM and TGSS data are equal to $\overline{F/F_{sp,\,old}} = 1.13 \pm 0.48$ and 1.05, respectively.

We also chose the sources with reliable fitted spectra at high and low frequencies. We put into this category the objects with available flux measurements made at more than two frequencies, signal-to-noise ratio $S/N > 5$, available data in the GB6 catalog, and no blending. In this sample, which includes about one third of all objects of the list, $\overline{F/F_{sp}} = 0.95 \pm 0.19$ the median ratio is 0.97 and $\overline{F/F_{sp,\,old}} = 0.95 \pm 0.18$ with the median equal to 0.95.

Figure 4a shows the histogram of the distribution of F/F_{sp} for the entire sample and for sources with reliable fluxes (the gray zone) for the entire sample and for sources with reliably determined fluxes (the gray bars). Figure 4b shows similar distributions for $F/F_{sp,\,old}$.

For sources with flux density measurements available only at 1.4 and 3.94 GHz and/or $S/N < 5$, we found $\overline{F/F_{sp}} = 1.17 \pm 0.43$ and the median 1.09 (13% of the sources) and $\overline{F/F_{sp,\,old}} = 1.17 \pm 0.36$ and the median 1.07 (58% sources).

Thus the observed fluxes agree quite well with the expected fluxes, and this fact, combined with the $\overline{RA}$ values determined from scans, confirms the reliability of the detection of studied sources on averaged scans.

5.3. Area Covered by the RCR Catalog

When locating RCR sources we refined the area covered by the catalog. To this end, the minimum and maximum coordinates for each hour interval of right ascension were determined. The average extent of the area where RCR sources were detected, for each hour in right ascension and declination was equal to :

$$\overline{\Delta RA} = 54^m.6 \pm 1^m.2, \quad \overline{\Delta Dec} = 33'.4 \pm 7'.2.$$

For such $\overline{\Delta RA}$ the gaps at the beginning of each hour[4], appear to cover 2^m. The maximum width of the survey strip from the location of sources for the interval of $2^h \le RA < 7^h$ is 43′.4.

Figure 5 shows the distribution of deviations ΔDec of RCR sources in declination from the central section for all sources of the catalog (the empty bars) and for the other samples (the gray bars). Figure 5a shows the distribution for faint sources,

[4] In the first paper about RCR catalog [10] the calibration time of the radiometer at the beginning of every observational hour is pointed as 1^m.

for which $F \leq 17.5$ mJy, Fig. 5b—shows the corresponding plot for bright sources ($F > 60$ mJy) ($17.5 < F \leq 60$ mJy), and Fig. 5c, the plot for bright sources($F > 60$ mJy).

The sensitivity of the power-beam pattern of RATAN-600 decreases from the center outwards. In the central part of the diagram fainter sources can be seen, whereas strong sources can be recorded also near the boundary of the field of view of the radio telescope. It is evident from Fig. 5 and Table 2 that surveys have zones with different detection threshold because of the feature of the power-beam pattern. Three zones of object can be identified [34]. In the first ($13'$ wide) zone at 3.94 GHz sources weaker than 17.5 mJy are detected, in the second $29'$-wide zone, sources weaker than 60 mJy are seen, and in the third, about $44'$-wide strip, sources brighter than 60 mJy are detected.

For $\overline{\Delta \mathrm{RA}} = 58^{\mathrm{m}}$ and $\overline{\Delta \mathrm{Dec}} = 43.'4$ the survey area for each hour and for bright sources turned out to be $10.5\,\square^\circ$, For example, we have for the entire range of right ascensions $2^{\mathrm{h}} \leq \mathrm{RA} < 7^{\mathrm{h}}$—$52.5\,\square^\circ$. For intermediate-brightness sources the area covered by the strip is smaller — $37\,\square^\circ$, or about 65% of the total area covered by the survey. The corresponding area for weak sources is $16\,\square^\circ$, or 30%.

6. CONCLUSIONS

As a result of our reduction of observations made at RATAN-600 radio telescope in the sky strip at the declination of SS 433 ($\mathrm{Dec}_0 \approx 5^\circ$) during the period from 1987 to 1999, and reprocessing of the data of the "Cold-80" survey (1980–1981) in the right-ascension interval $2^{\mathrm{h}} \leq \mathrm{RA} < 7^{\mathrm{h}}$ we obtained a list of radio sources extending the RCR catalog. We identified all sources with objects of the NVSS catalog. We found a total of 237 sources including 20 blends, 8 double sources, and three sources with three NVSS components.

We determined the integrated flux densities at 3.94 GHz and right ascensions of the radio sources from averaged scans. We did not determine the declinations for detected sources but used the declinations of the NVSS objects identified with these sources.

We determined the spectral indices at 0.5 and 3.94 GHz for each object of the list. To construct the spectra, we used all information about integrated fluxes at different frequencies available via CATS, VizieR, and NED resources, as well as flux density estimates obtained from VLSSr, GLEAM, TGSS, and GB6 survey maps. These estimates were primarily useful for constructing the spectra of sources with flux data available only at two frequencies: 3.94 GHz (RCR) and 1.4 GHz (NVSS). These are usually sources with flux densities lower than 30 mJy, and 87% of them have flat or inverted spectra ($\alpha > -0.5$).

We constructed the histograms and plots of the distribution of spectral indices at 0.5 and 3.94 GHz (Figs. 1 and 2). At first we used mostly VLSSr and TXS survey data for constructing the spectra in the low-frequency range, then added the data from the new low-frequency surveys GLEAM and TGSS, which are one order of magnitude more sensitive than VLSSr and TXS. We compared the spectral indices and shapes of the radio spectra for the sources of the list incorporating the data from new low-frequency sky surveys and without these data. The form of the distributions $\alpha_{3.94}$ and $\alpha_{0.5}$ changed (Fig. 1), the number of sources with steep spectra increased by about 10%.

Soboleva et al. [10] considered six types of radio spectra: S, C^-, C^+, spectra with a maximum (MPS, GPS, HFP) and minimum ("upturn") at a certain frequency, and spectra with a more complex shape ("hill"). We also used this classification and found that incorporating new GLEAM and TGSS data decreased the number of spectra approximated by straight line (S) by 10%, decreased slightly the number of C^- spectra (by 4%), increased the number of sources with C^+ spectra by 4%, and increased the number of sources with upturn spectra from 3 to 16. These changes are due to observational selection. To take it into account in the classification of sources according to the shape of the spectrum, we need the flux data in the high-frequency range 4–15 GHz.

We validated the reliability of the resulting list of radio sources by first cross-identifying it with the NVSS survey whose angular resolution is close that of the "Cold" surveys, and then with the FIRST and TGSS surveys. We also compared the right ascensions of NVSS sources with the right ascensions determined from averaged scans (Fig. 3 and Table 2) and the ratio of the integrated flux densities measured at 3.94 GHz to the expected fluxes computed from radio spectra (Fig. 4). This comparison confirmed the reliability of detection of the sources studied on averaged scans.

We refined the area covered by the survey in the right-ascension interval considered. The sensitivity of the RATAN-600 power-beam pattern is known to decrease from the center toward the boundaries. Weaker sources are observed in the central part of the survey, whereas strong sources are detected at the boundary of the field of view of the radio telescope. Three survey zones can be selected. In the central zone with the width of about $13'$ sources weaker than 17.5 mJy are detected, in the second zone with the width of about $29'$ sources with fluxes below 60 mJy are detected, and brighter sources are detected in

about 44′ wide strip. In accordance with these thresholds the survey covers 16, 37, and 52.5 □°, respectively, in the right-ascension interval considered.

The sky surveys of the "Cold" experiment [1–4], carried out on RATAN-600 radio telescope from 1980 to 1999 provide more complete information about spectral indices of decimeter-way sources. They constitute an intermediate link between deep VLA surveys at 1.4 GHz and low-sensitivity all-sky surveys. In the right-ascension interval considered we found no objects that were not included into decimeter-wave catalogs, at least at the 10–15 mJy level.

ACKNOWLEDGMENTS

This work was supported in part by the Russian Foundation for Basic Research (grant no. 14-07-00361). Observations with the RATAN-600 radio telescope are carried out with the financial Support of the Ministry of Education and Science of the Russian Federation (state contract 14.518.11.7054).

REFERENCES

1. Y. N. Pariiski, N. N. Bursov, N. M. Lipovka, et al., Astron. and Astrophys. Suppl. **87**, 1 (1991).
2. Y. N. Pariiskii and D. V. Korolkov, Itogi Nauki i Tekhniki Seriia Astronomiia **31**, 73 (1986).
3. A. B. Berlin, E. V. Bulaenko, V. Y. Golnev, et al., Soviet Astronomy Letters **7**, 161 (1981).
4. Y. N. Parijskij and D. V. Korol'kov, Astrophys. Space Physics Reviews **5**, 39 (1987).
5. J. J. Condon, W. D. Cotton, E. W. Greisen, et al., Astron. J. **115**, 1693 (1998).
6. R. L. White, R. H. Becker, D. J. Helfand, and M. D. Gregg, Astrophys. J. **475**, 479 (1997).
7. O. P. Zhelenkova, Candidate's Dissertation in Mathematics and Physics (SAO RAS, Nizhnij Arkhyz, 2007).
8. O. P. Zhelenkova and A. I. Kopylov, Astrophysical Bulletin **63**, 346 (2008).
9. N. S. Soboleva, N. N. Bursov, and A. V. Temirova, Astronomy Reports **50**, 341 (2006).
10. N. S. Soboleva, E. K. Majorova, O. P. Zhelenkova, et al., Astrophysical Bulletin **65**, 42 (2010).
11. F. Bonnarel, P. Fernique, O. Bienaymé, et al., Astron. and Astrophys. Suppl. **143**, 33 (2000).
12. T. Boch and P. Fernique, ASP Conf. Ser. **485**, 277 (2014).
13. M. B. Taylor, ASP Conf. Ser. **347**, 29 (2005).
14. N. S. Soboleva, A. V. Temirova, and N. N. Bursov, Report SPb Branch SAO RAS, Vol. 2 (St. Petersburg Branch of the Special Astrophysical Observatory of RAS, St. Petersburg, 2008).
15. E. K. Majorova, Bull. Spec. Astrophys. Obs. **53**, 78 (2002).
16. O. V. Verkhodanov, S. A. Trushkin, H. Andernach, and V. N. Chernenkov, ASP Conf. Ser. **125**, 322 (1997).
17. O. V. Verkhodanov, S. A. Trushkin, H. Andernach, and V. N. Chernenkov, Bull. Spec. Astrophys. Obs. **58**, 118 (2005).
18. F. Ochsenbein, P. Bauer, and J. Marcout, Astron. and Astrophys. Suppl. **143**, 23 (2000).
19. A. S. Cohen, W. M. Lane, W. D. Cotton, et al., Astron. J. **134**, 1245 (2007).
20. W. M. Lane, W. D. Cotton, S. van Velzen, et al., Monthly Notices Royal Astron. Soc. **440**, 327 (2014).
21. P. C. Gregory, W. K. Scott, K. Douglas, and J. J. Condon, Astrophys. J. Suppl. **103**, 427 (1996).
22. R. B. Wayth, E. Lenc, M. E. Bell, et al., Publ. Astron. Soc. Australia **32**, e025 (2015).
23. N. Hurley-Walker, J. R. Callingham, P. J. Hancock, et al., Monthly Notices Royal Astron. Soc. **464**, 1146 (2017).
24. H. T. Intema, P. Jagannathan, K. P. Mooley, and D. A. Frail, Astron. and Astrophys. **598**, A78 (2017).
25. O. V. Verkhodanov, ASP Conf. Ser. **125**, 46 (1997).
26. G. Miley and C. De Breuck, Astron. Astrophys. Rev. **15**, 67 (2008).
27. E. K. Majorova, O. P. Zhelenkova, and A. V. Temirova, Astrophysical Bulletin **70**, 33 (2015).
28. J. N. Douglas, F. N. Bash, F. A. Bozyan, et al., Astron. J. **111**, 1945 (1996).
29. C. P. O'Dea, Publ. Astron. Soc. Pacific **110**, 493 (1998).
30. S. Tinti and G. de Zotti, Astron. and Astrophys. **445**, 889 (2006).
31. S. Tinti, D. Dallacasa, G. de Zotti, et al., Astron. and Astrophys. **432**, 31 (2005).
32. W. A. Dent and F. T. Haddock, Nature **205**, 487 (1965).
33. M. Tucci, J. A. Rubiño-Martin, R. Rebolo, et al., Monthly Notices Royal Astron. Soc. **386**, 1729 (2008).
34. O. P. Zhelenkova, N. S. Soboleva, E. K. Majorova, and A. V. Temirova, Astrophysical Bulletin **68**, 26 (2013).

Translated by A. Dambis